Supporting information for

Hydrogen Peroxide and Dioxygen Activation by Dinuclear Copper Complexes in Aqueous Solution: Hydroxyl Radical Production Initiated by Internal Electron Transfer

Qing Zhu,† Yuxiang Lian, ‡ Sunita Thyagarajan,‡ Steven E. Rokita,†
Kenneth D. Karlin*‡ and Neil V. Blough*,†

†*Department of Chemistry and Biochemistry, University of Maryland, College Park, Maryland 20742*

‡*Department of Chemistry, Johns Hopkins University, Baltimore, Maryland 21218*

E-mail: neilb@umd.edu; karlin@jhu.edu; rokita@umd.edu

Content

Hydroxyl radical detection through trapping of the methyl radical in the presence of DMSO or methane

Radical trapping experiments employed 5 ml Micro-Vials in a total reaction volume of 3 ml. A sample solution containing $Cu^{II}_2N_{4,5}$ (10 μM), DMSO (1.5 mM) and 3-ap (50 μM) was prepared in 10 mM phosphate buffer at pH 6.8. The solution was deoxygenated by bubbling with ultra-high purity nitrogen gas for 20 minutes before the reaction was initiated by addition of a solution of deoxygenated H_2O_2 (100 μM). The reaction solution was purged with N_2 during the entire course of the reaction to maintain anaerobic conditions. The reaction was terminated at different times by withdrawal of an aliquot (100 μL) and derivatization with fluorescamine under aerobic conditions. Derivatization was performed as follows: the 100 μL of the reaction mixture was mixed with 400 μL borate buffer (0.2 M, pH 8.4); 200 μL of fluorescamine (5 mM) in acetonitrile were then

added to the product, Me-3ap (I), to produce Me-3apf (III) (Scheme S1).[1-3] The resultant solution was vortexed and kept in the dark for 3 minutes to complete the reaction before sample loading onto the HPLC (reversed-phase) for separation and quantification. The mobile phase composition was 35% sodium acetate buffer (50 mM, pH 4.0)/ 65% methanol (v/v). The excitation and emission wavelengths on the fluorometric detector were set to 390 nm and 490 nm, respectively, with quantification performed as described previously.[2-5] The time-dependence of Me-3apf formation for the $Cu^{II}_2\mathbf{N}_5$ complex in the presence of DMSO is provided in Figure S1.

As a further test for the production of the hydroxyl radical, methane was used in place of DMSO. The sample solution, containing $Cu^{II}_2\mathbf{N}_{4,\,5}$ (10 μM) and 3-ap (20 μM), was purge with methane for 20 minutes (the concentration of methane in a saturated aqueous solution at room temperature is 1.5 mM[6]). A deoxygenated solution of H_2O_2 (100 μM) was then added to the sample solution to initiate the reaction. Methane was used to purge the reaction solution during the timecourse of the reaction to maintain anaerobic conditions. The reaction was terminated at different times by derivatization with fluorescamine under aerobic conditions, with separation and quantitation performed as described above. The time dependence of Me-3apf formation for the $Cu^{II}_2\mathbf{N}_5$ complex in the presence of methane is provided in Figure S1.

Above 20 μM 3-ap, the yield of Me-3apf decreased with increasing [3ap] (Figure S2), consistent with a direct competitive reaction of 3ap with the intermediate (see further below). A lower 3-ap concentration (20 μM) was thus employed initially in the methane experiments to maximize yield (Figure S1, S2).

The substantial reduction in Me-3apf yield in the presence of 1.5 mM methane as compared to the presence of 1.5 mM DMSO (Figure S1) can be attributed to the substantial difference in the rate constants for reaction of OH with these compounds (Table S1); because the rate constant for reaction of methane with OH is far smaller than that for DMSO, competitive reaction of OH with other solution constituents is expected in the presence of methane. For DMSO, the yield of Me-3apf (Y_{DMSO}) can be approximated by the following expression,

$$Y_{DMSO} = \frac{Y_0\, k_{DMSO}[DMSO]}{k_{DMSO}[DMSO] + k_{3\text{-}ap}[3\text{-}ap] + k_{H_2O_2}[H_2O_2] + k_{Cu}[Cu\ complex]} \qquad (1)$$

where Y_0 is the yield of hydroxyl radical and k_{DMSO}, $k_{3\text{-ap}}$, k_{Cu} and k_{H2O2} are rate constants for reaction of the OH radical with DMSO[7], 3-ap[8,9], the Cu(II) complex and H_2O_2[8] respectively (Table S1). Because of the large rate constant for reaction of DMSO with OH (Table S1), k_{DMSO} [DMSO]>> ($k_{3\text{-ap}}$[3-ap] + k_{H2O2}[H_2O_2] + k_{Cu}[Cu complex]) and Eqn. 1 reduces effectively to $Y_{DMSO} = Y_0$. In contrast, the yield of Me-3apf in the presence of methane (Y_{CH4}) is given by,

$$Y_{CH_4} = \frac{Y_0 k_{CH_4}[CH_4]}{k_{CH_4}[CH_4] + k_{3\text{-ap}}[3\text{-ap}] + k_{H_2O_2}[H_2O_2] + k_{Cu}[\text{Cu complex}]} \quad (2)$$

where k_{CH4} is rate constant for reaction of OH radical with methane; because of the small value of k_{CH4} (Table S1),[7,10] the product, $k_{CH4}[CH_4]$, does not dominate the other terms in the denominator of Eqn. 2 under the conditions of this experiment (Fig. S1), and thus a lower yield is anticipated.

To examine whether the reduction in yield in the presence of CH_4, relative to that in the presence of DMSO, was consistent with that of OH as the reactive intermediate, the ratio of Me-3apf yields in DMSO to that in methane was determined ($Y_{DMSO}/Y_{methane}$ = 2.8 ± 0.4 for $Cu^{II}_2\mathbf{N_4}$ complex and $Y_{DMSO}/Y_{methane}$ = 2.9 ± 0.2 for $Cu^{II}_2\mathbf{N_5}$ complex; see Fig 3A and Fig. S1) and compared with the predicted ratio (R),

$$R = \frac{Y_{DMSO}}{Y_{CH_4}} = 1 + \frac{k_{3\text{-ap}}[3\text{-ap}] + k_{H_2O_2}[H_2O_2] + k_{Cu}[\text{Cu complex}]}{k_{CH_4}[CH_4]} \quad (3)$$

Because the rate constant for reaction of OH with the Cu complexes was unknown, we initially assumed that the intermediate was not reactive with the Cu complexes (relative to the reaction with 3-ap and H_2O_2). However, based on this assumption, the predicted yield ratio (R≈1.7) was significantly lower than those determined experimentally (see above and Fig. S1), indicating that the Cu complexes also reacted rapidly with the intermediate. To estimate the rate constant for reaction of the intermediate with the Cu complexes, Eqn. 3 was rearranged to solve for k_{Cu}, using the concentrations of reactants provided in Fig. S1 and employing the rate constants for reaction with OH provided in Table S1. The estimated rate constant for k_{Cu} was at or very near the diffusion-limited value, $2.2\text{x}10^{10}$ $M^{-1}s^{-1}$, consistent with a reaction of OH. Further, doubling the concentration of 3-ap to 40 μM increased R to ~3.3 as expected

(Fig. S1, S2), while still providing a similar estimate for k_{Cu} (2.1×10^{10} $M^{-1}s^{-1}$), furnishing further evidence for OH as the intermediate. These results, combined with the observed reactivity with DMSO, CH_4, and benzoic acid (see below), provide exceedingly strong evidence that the detected intermediate is indeed OH.

Quantitative determination of hydroxyl radical yields in the presence and absence of catalase

Quantitative determinations of OH yield were obtained in the presence of higher concentrations of DMSO (10 mM) and 3-ap (500 μM) to ensure unequivocally complete reaction with the OH and methyl radical, respectively. As above, the experiments were carried out in a 5 ml Micro-Vial with total reaction volume of 3 ml. A sample solution containing $Cu^{II}_2\mathbf{N_{4,5}}$ complex (20 μM), DMSO and 3-ap was prepared in 10 mM phosphate buffer at pH 6.8. The solution was deoxygenated by bubbling with ultra-high purity nitrogen gas for 20 minutes before the reaction was initiated by addition of deoxygenated solution of H_2O_2 (80 μM). The reaction solution was purged with N_2 during the entire course of the reaction. Catalase was absent or added when the intermediate formation was complete. The reaction was terminated at different times by derivatization with fluorescamine under aerobic conditions. The analysis of Me-3apf was performed as described above. Results for $Cu^{II}_2\mathbf{N}_4$ and $Cu^{II}_2\mathbf{N}_5$ are shown in Figures S3 and S4, respectively.

Hydroxyl radical determination through reaction with benzoic acid

Benzoic acid was used to determine hydroxyl radical yield under aerobic conditions. The reaction solution, containing benzoic acid (1.0 mM) and Cu(II) complex (10.0 μM), was prepared in phosphate buffer (10 mM, pH 6.8). This solution was purged with air for 20 minutes before H_2O_2 (6.0 mM) was added to initiate the reaction. The reaction was terminated at different times by directly injecting the sample into the reversed-phase HPLC and detecting the formation of salicylic acid fluorometrically. Because the ratio of three hydroxylated isomers, 2-OH-BA, 3-OH-BA and 4-OH-BA, is close to 1:1:1 (Scheme S2),[11] the yield of hydroxyl radicals generated in the reaction was approximated as three times the concentration of salicylic acid quantified by HPLC. For

separation and identification of salicylic acid, the mobile phase composition was 65% phosphate buffer (25 mM, pH 2.0)/ 35% methanol (v/v). The excitation and emission wavelengths were set to 305 nm and 410 nm, respectively, on the fluorescence detector.[11] A comparison between the results obtained for $Cu^{II}_2\mathbf{N}_4$ and $Cu^{II}\mathbf{N}$ is provided in Figure S5.

Ligand degradation products analysis

Product analysis by thin layer chromatography

Thin layer chromatography (TLC) was employed for a preliminary analysis of the products formed from reaction of Cu(II) complexes with H_2O_2. $Cu^{II}_2\mathbf{N_4}$ complex (2 mM) and H_2O_2 (7 mM), dissolved in 10 mM phosphate buffer at pH 6.8, were mixed rapidly to initiate the reaction under anaerobic conditions. The resulting solution was allowed to react for 15 minutes at room temperature; concentrated ammonium hydroxide (~250 μL) was then added to release the ligands, which were then extracted into a minimum volume of methylene chloride. The extraction was loaded onto a 10×20 cm silica gel thin layer chromatography plate (AnalTech, Inc) and developed using a mobile phase containing methanol and concentrated ammonium hydroxide v/v, 100:5. After drying, the TLC plate was placed into a container containing iodine vapor for visualization of the products. For $Cu^{II}_2\mathbf{N}_4$, three products, with R_f values distinct from the original ligand, were observed to be formed (Table S2).

Because the absorption spectra of the products produced in the absence and presence of OH scavengers (glucose, DMSO) were observed to differ significantly (data not shown), we also investigated the effect of the presence of DMSO on product distribution. $Cu^{II}_2\mathbf{N_4}$ complex (2 mM) and DMSO (2 M) were prepared in phosphate buffer (10 mM, pH 6.8) prior to addition of H_2O_2 (7 mM). Other experimental procedures and the TLC analysis were identical to those performed in the absence of DMSO. In this case, one of the reaction products was no longer observed (Table S2), suggesting that OH generated from the decay of intermediate was also reacting in part with the complexes to form an additional product.

Synthetic level isolation and identification of ligand degradation products

Ligand degradation products were also separated by column chromatography and characterized by ^{1}H-NMR and ^{13}C-NMR spectroscopies and ESI-MS in order to confirm the nature of ligand derived oxidation product.

$Cu^{II}_2\mathbf{N_4}$ (0.212 g (0.192 mmol) was dissolved in 30 mL air-free water. Then the Cu solution was transferred by cannula to a 100 mL phosphate buffer which was made by dissolving 0.355 g (2.50 mmol) of Na_2HPO_4 and 0.300 g (2.50 mmol) of NaH_2PO_4 in 100 mL air free water (25.0 mM, pH=6.8). With the solution at 0 ^{o}C (ice bath), 30 mL of a H_2O_2 solution (0.838 mmol) was injected to the Cu solution. The peroxide solution was made by dissolving 0.057 g 50 % H_2O_2 (aq) in 30 mL degassed water. The resulting reaction mixture was allowed to stir at 0 ^{o}C overnight. After that, excess $Na_2H_2EDTA{\bullet}2H_2O$ was added to the solution to remove the copper ion from complex. After overnight stirring, the resulting solution was extracted using 3×250 mL dichloromethane. The organic layer was collected and dried over magnesium sulfate, whereupon rotoevaporation lead to the isolation of total amount 0.081 g of organic material (i.e., 83 % recovery of all possible organic products). Column chromatography using silica gel was carried out starting with MeOH/1%-$NH_4OH_{(conc)}$ as eluent, with gradual increasing to MeOH/30%-NH_4OH. In addition to the original unreacted $\mathbf{N_4}$ ligand, three new significant components could be observed using TLC. Details, i.e., R_f values yields and spectroscopic data are given just below (Table S2). ^{1}H-NMR and ^{13}C-NMR spectra were recorded on a Bruker AF 400 FT-NMR instrument at room temperature. Chemical shifts (ppm) were referenced either to an internal standard (Me_4Si) or to residual solvent peaks. ESI mass spectra were acquired using a Finnigan LCQDeca ion-trap mass spectrometer equipped with an electrospray ionization source (Thermo Finnigan, San Jose, CA). Samples were injected through a syringe with the rate at 10 uL/min via a silica capillary line. The heated capillary temperature was 250 °C and the spray voltage was 5 kV. We provide below the structure of major components together with their yields (by weighing).

Major Component: This component was isolated in a yield of 28 %, $R_f = 0.53$ (also see Table S2). Figure S6 gives the structure assigned for this major component, based on ^{1}H

NMR, ^{13}C NMR and ESI-MS. The data are: ^{1}H-NMR (CDCl3): δ 1.6–1.7 (m, 4 H), 2.7-2.8 (m, 6 H), 2.8-2.9 (s, 2H), 3.0-3.1 (s, 10 H), 7.0-7.3 (m, 8H), 7.5-7.6 (m, 4H), 8.4-8.5 (m, 4H). ^{13}C-NMR (CDCl3): δ 24.1, 33.4, 46-47, 54.3, 121-122, 123.8, 137.0, 149.2, 157.9, 167.3. ESI-MS: (523.52, M+H$^+$). (Figure S6)

Minor Component I: This was obtained in 15 % yield, R_f = 0.66 (see Table S2). Proposed structures for this minor component are given in Figure S7 based on the ESI-MS result, m/z 525.57, (M+H$^+$). Absolute structural confirmation cannot be made since the ^{1}H-NMR and ^{13}C-NMR spectroscopic data suggest component I is a mixture.

Minor Component II: Here, the yield is only ~ 10% and R_f = 0.40, which was not directly observed in the initial TLC analyses. Figure S8 gives the possible structure of this component from based on ^{1}H-NMR and ESI-MS characterization. ^{1}H-NMR ($CDCl_3$): δ 1.4-1.5 (m, 4 H), 2.5-2.6 (m, 4 H), 2.6-2.7 (m, 2H), 2.9-3.0 (m, 6 H), 2.9-3.0 (m, 4 H), 7.0-7.2 (m, 6H), 7.5-7.6 (m, 3H), 8.5-8.6 (m, 3H). ESI-MS: (m/z 404.28, M+).

For the $\mathbf{N_5}$ containing complex $Cu^{II}_2\mathbf{N_5}$, nearly identical procedures were employed to isolate the ligand derived oxidation product. Here, the total yield of isolated organics was 0.120 g (48 % recovered). Column chromatography was similarly carried but the solvent mixture only varied over 1 % to 4 % $NH_4OH_{(conc)}$ in MeOH.

Major component: The major component of ligand degradation products gives an R_f = 0.85, with a total yield of 69%. From the combined spectroscopies, the product assigned is as shown in Figure S9. ^{1}H-NMR ($CDCl_3$): δ 1.2–1.3 (m, 2H), 2.1-2.2 (m, 2H), 2.6-2.7 (m, 2H), 2.9-3.0 (s, 12H) , 3.6-3.7 (m, 1H) , 4.9-5.1 (m, 2H) , 5.7-5.8 (m, 1H), 7.0-7.2 (m, 8H), 7.5-7.6 (m, 4H), 8.5-8.6 (m, 4H). ^{13}C-NMR ($CDCl_3$): δ 34.3, 36-37, 53-54, 93.1, 115-116, 121-122, 123.7, 136.8, 139.0, 149.5, 161.0. ESI-MS: (m/z 282.15, (M+2Na)/2).

Minor component: Here, the R_f = 0.54 (yield ~10%). Possible structures of this minor component are given in Figure S9 based on the ESI-MS result, (m/z, 543.32 (M+Na$^+$). However, this component appears to be a mixture.

EPR Spectroscopic Characterization.

Electron paramagnetic resonance (EPR) spectra were recorded on a Bruker EMX spectrometer controlled with a Bruker ER 041 X G microwave bridge operating at X-band (~9.4 GHz). A 'flat-cell' sample holder for aqueous RT measurements was employed and $[Cu^{II}(TMPA)(H_2O)](ClO_4)_2$ was used as an internal standard[12] to compare intensities and thus relative concentrations. Instrument settings were as follows: Receive Gain, 4.48e+4; Modulation.Amplitude, 2.00G; Frequency, 9.701882 GHz; Power, 6.346 mW.

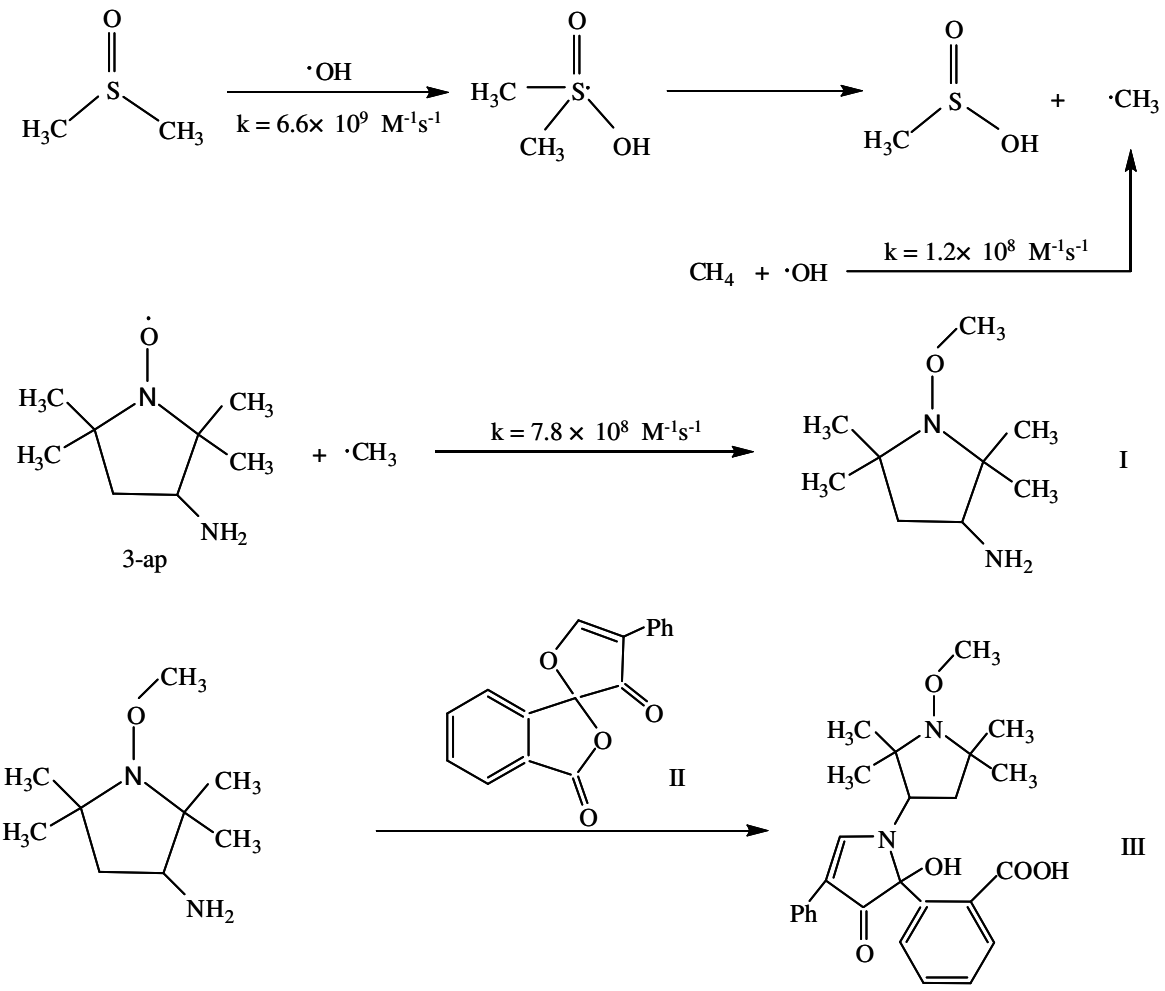

Scheme S1. Reaction scheme for the detection of the methyl radical in the presence of DMSO or methane.

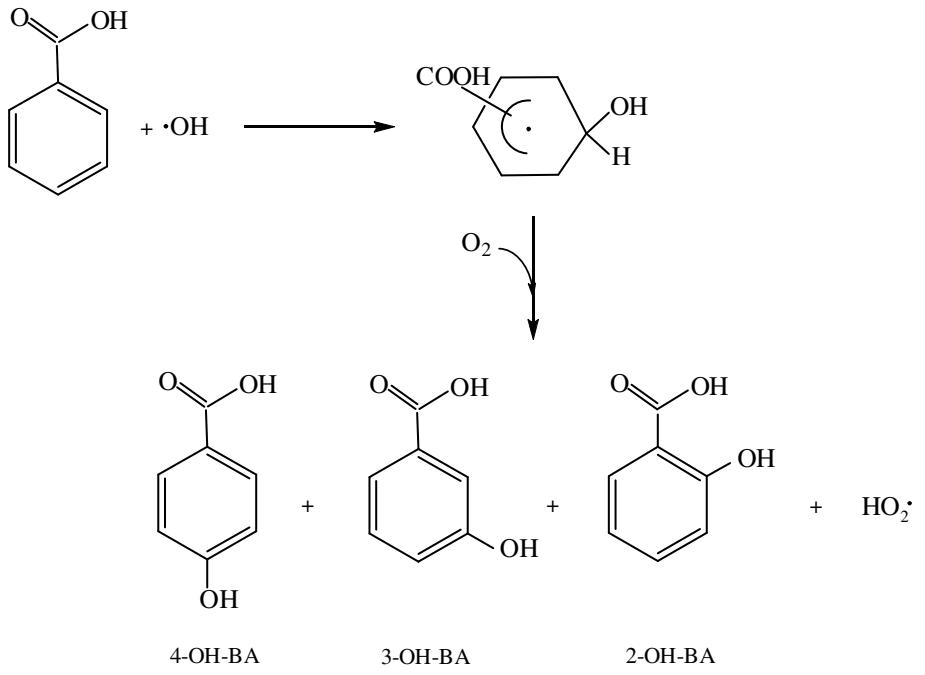

Scheme S2. Reaction scheme for the detection of the hydroxyl radical in the presence of benzoic acid.

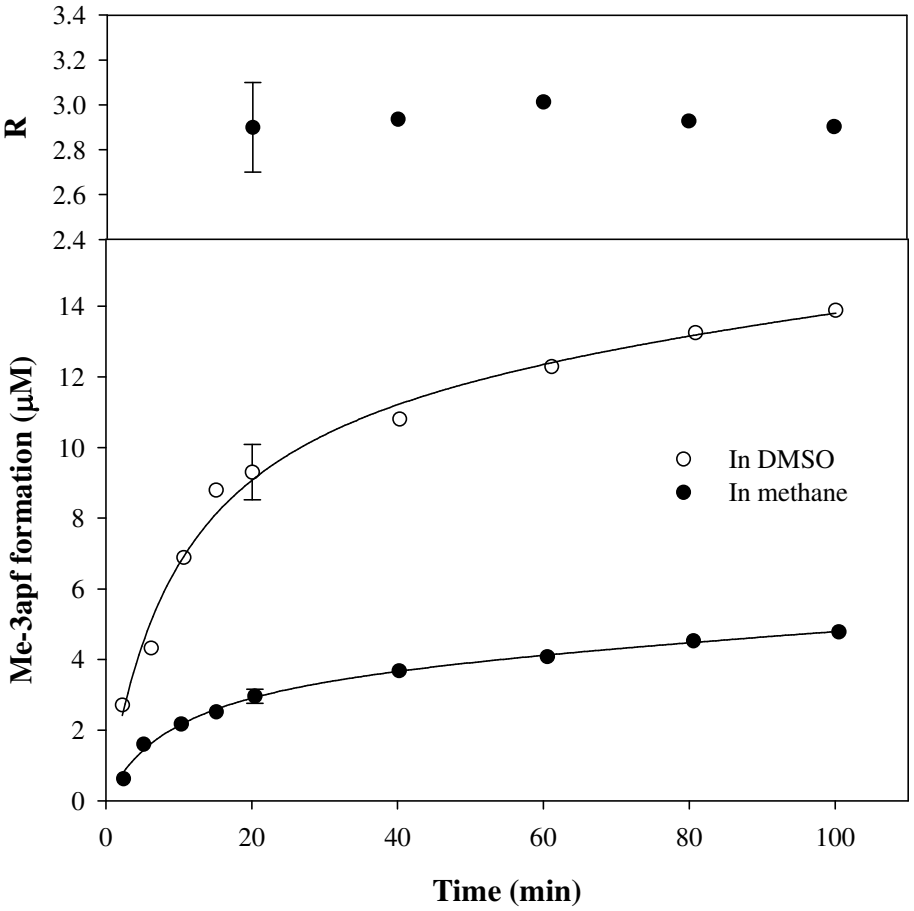

Figure S1. Me-3apf formation in the presence of DMSO or methane. In the DMSO experiment, $Cu^{II}_2\mathbf{N_5}$ complex (10.0 μM), DMSO (1.5 mM) and 3-ap (50 μM) were dissolved in phosphate buffer (10 mM, pH 6.8). H_2O_2 (100 μM) was added to initiate the reaction under anaerobic conditions. In the methane experiment, $Cu^{II}_2\mathbf{N_5}$ complex (10.0 μM), methane (1.5 mM) and 3-ap (20 μM) was employed. Reaction was terminated at different times by derivatization with fluorescamine under aerobic conditions. Me-3apf was then separated and analyzed by reversed-phase HPLC. Lines in this figure were obtained from a fit to polynomial equation only to highlight the trend of Me-3apf formation. Error bars represent ±1 standard deviation about the mean of at least three independent experiments.

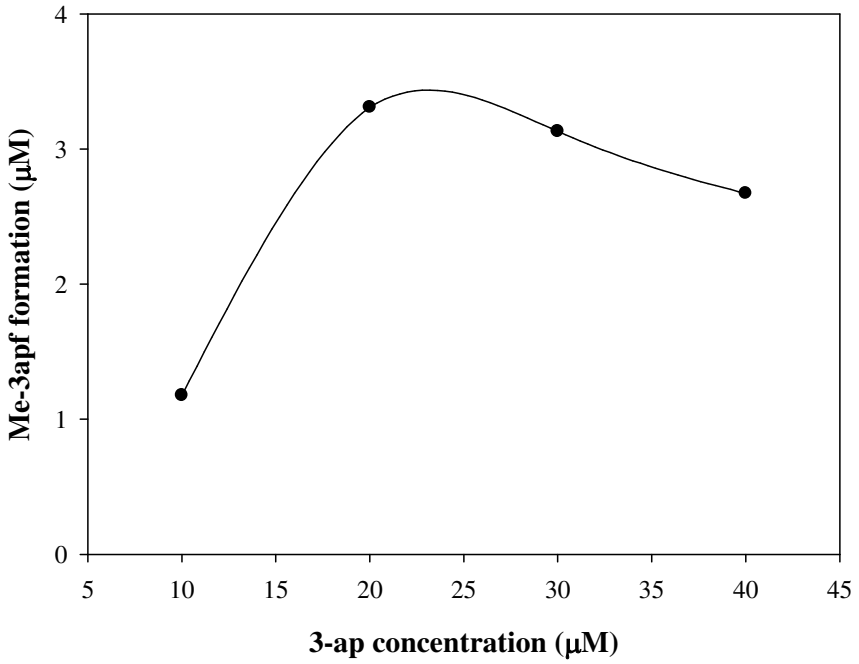

Figure S2. Dependence of Me-3apf formation on 3-ap concentration in the presence of methane. $Cu^{II}_2\mathbf{N_4}$ complex (10.0 μM), methane (1.5 mM) and 3-ap were combined in phosphate buffer (10 mM, pH 6.8). H_2O_2 (100 μM) was added to initiate the reaction under anaerobic conditions. Reaction was terminated after 20 minutes by derivatization with fluorescamine under aerobic conditions. Me-3apf was then separated and analyzed by reversed-phase HPLC.

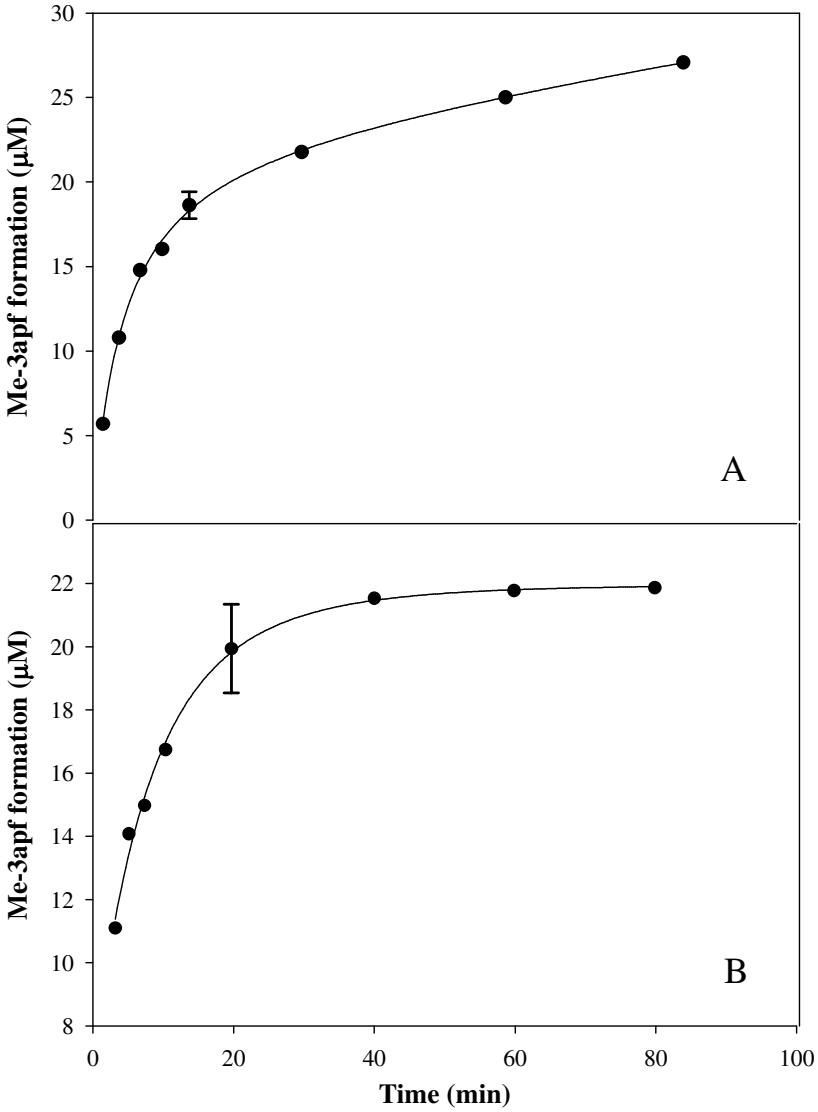

Figure S3. Me-3apf formation (OH yield) from $Cu^{II}_2\mathbf{N_4}$ in the presence and absence of catalase. $Cu^{II}_2\mathbf{N_4}$ complex (20.0 μM), DMSO (10 mM) and 3-ap (500 μM) were combined in phosphate buffer (10 mM, pH 6.8). H_2O_2 (80 μM) was then added to initiate the reaction under anaerobic conditions. Catalase was absent (Panel A) or added (1.5 units/ml; Panel B) when the intermediate formation was complete. Error bars represent ±1 standard deviation about the mean of at least three independent experiments.

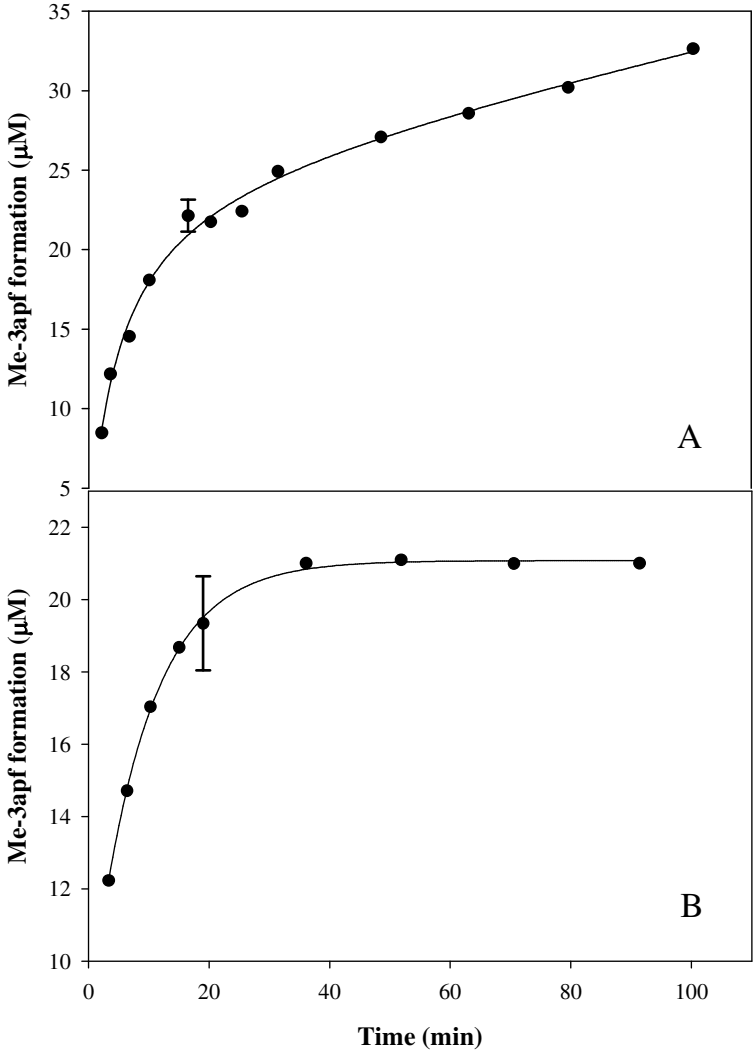

Figure S4. Me-3apf formation (OH yield) from $Cu^{II}_2\mathbf{N_5}$ in the presence and absence of catalase. $Cu^{II}_2\mathbf{N_5}$ complex (20.0 μM), DMSO (10 mM) and 3-ap (500 μM) were combinded in phosphate buffer (10 mM, pH 6.8). H_2O_2 (80 μM) was then added to initiate the reaction under anaerobic conditions. Catalase was absent (Panel A) or added (1.5 units/ml;Panel B) when the intermediate formation was complete. Error bars represent ±1 standard deviation about the mean of at least three independent experiments.

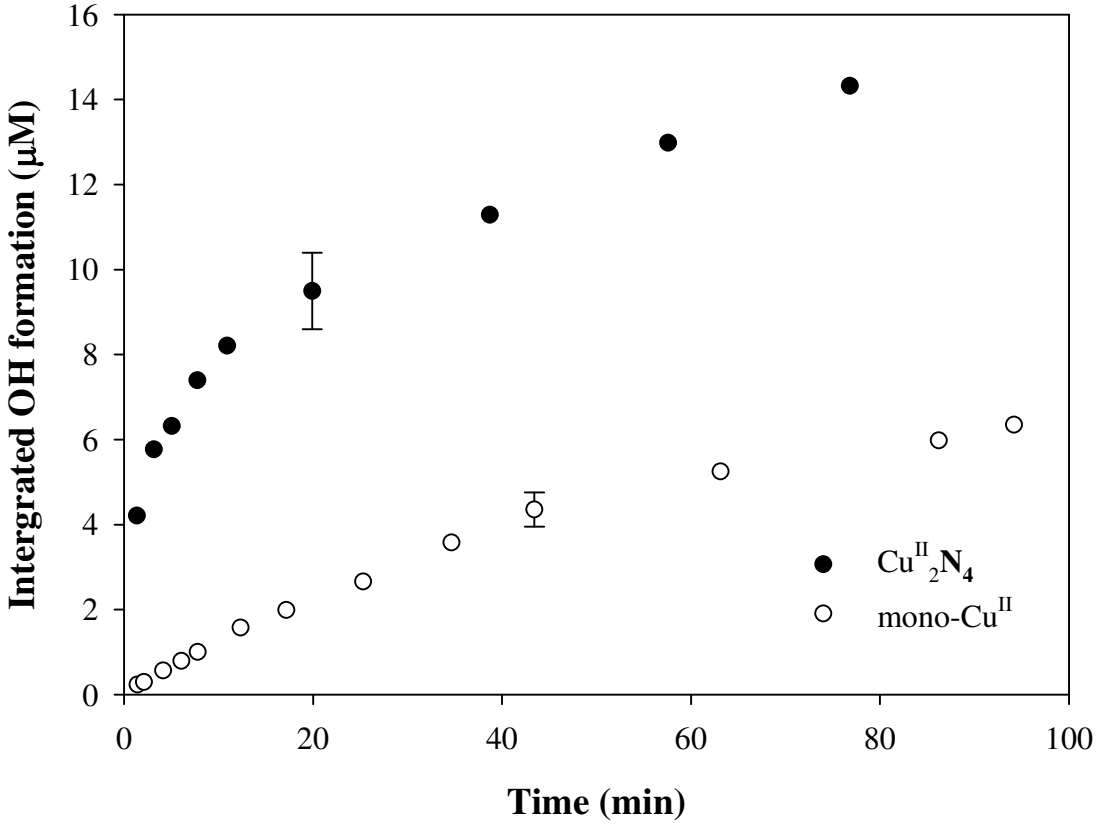

Figure S5. Hydroxyl radical yield from $Cu^{II}_2\mathbf{N_4}$ and $Cu^{II}\mathbf{N}$ employing benzoic acid under aerobic conditions. $Cu^{II}_2\mathbf{N_4}$ (10 μM) or $Cu^{II}\mathbf{N}$ (10 μM) and benzoic acid (1.0 mM) were combined in phosphate buffer (pH 6.8, 10 mM). H_2O_2 (6.1 mM) was added to initiate reaction under aerobic conditions. Reaction was terminated at different times by direct injection into HPLC. Formation of the hydroxyl radical was approximated as 3 times of the concentration of salicylic acid analyzed by HPLC. Error bars represent ±1 standard deviation about the mean of at least three independent experiments.

Table S1. Rate constants for hydroxyl radical reaction*

k_{DMSO}	$k_{3\text{-}ap}$	k_{H2O2}	k_{CH4}	k_{Cu}**
6.6×10^9	4.9×10^9	4.5×10^7	1.2×10^8	2×10^{10}

* See text for references
** Estimate from this work

Table S2. Product analysis by TLC in the presence and absence of an added OH scavenger

Sample	R_f1	R_f2	R_f3	R_f ligand
$Cu^{II}_2N_4$	/	/	/	0.88 ± 0.03
$Cu^{II}_2N_4 + H_2O_2$	0.22 ± 0.04	0.53 ± 0.06	0.66 ± 0.05	0.88 ± 0.03
$Cu^{II}_2N_4 + H_2O_2$ + DMSO	/	0.53 ± 0.06	0.66 ± 0.05	0.88 ± 0.03

R_f1-R_f3 are the retardation factors of the degradation products. The uncertainties in R_f represent ± one standard deviation from the average of three independent experiments.

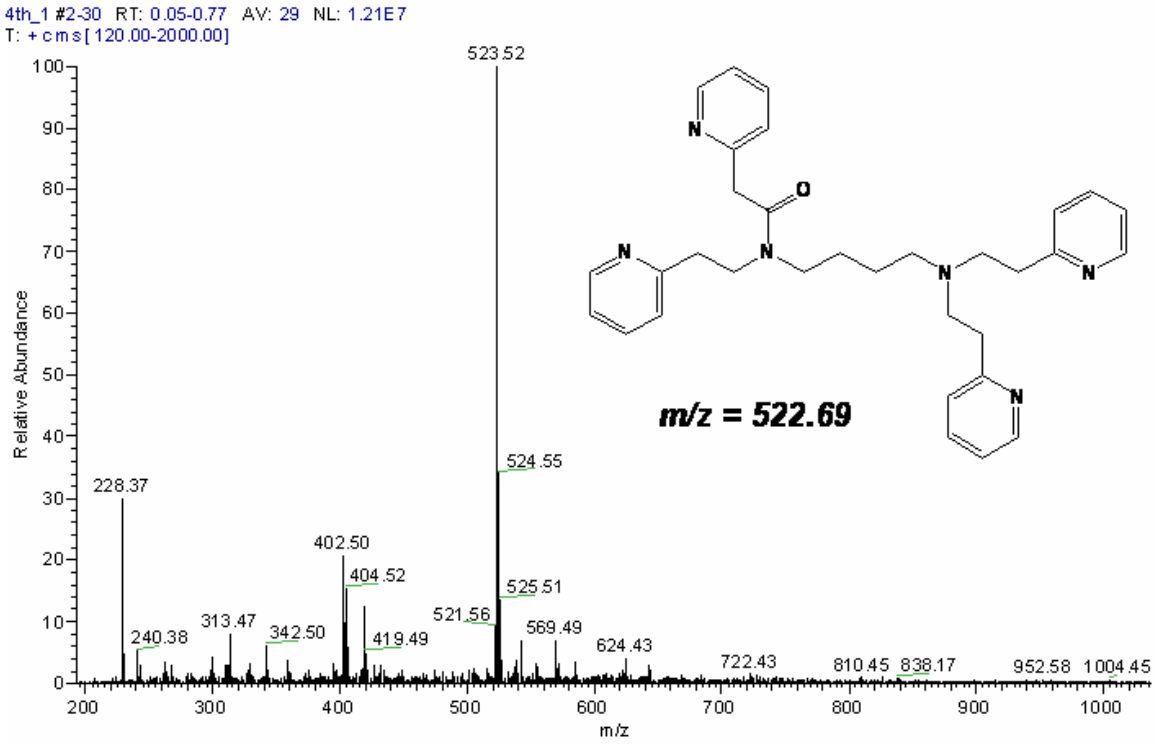

Figure S6. ESI-MS spectrum of the major component of ligand degradation products after $Cu^{II}_2\mathbf{N_4}$ reaction with H_2O_2. The insert shows the structure proposed, based on ^{1}H NMR, ^{13}C NMR and ESI-MS data.

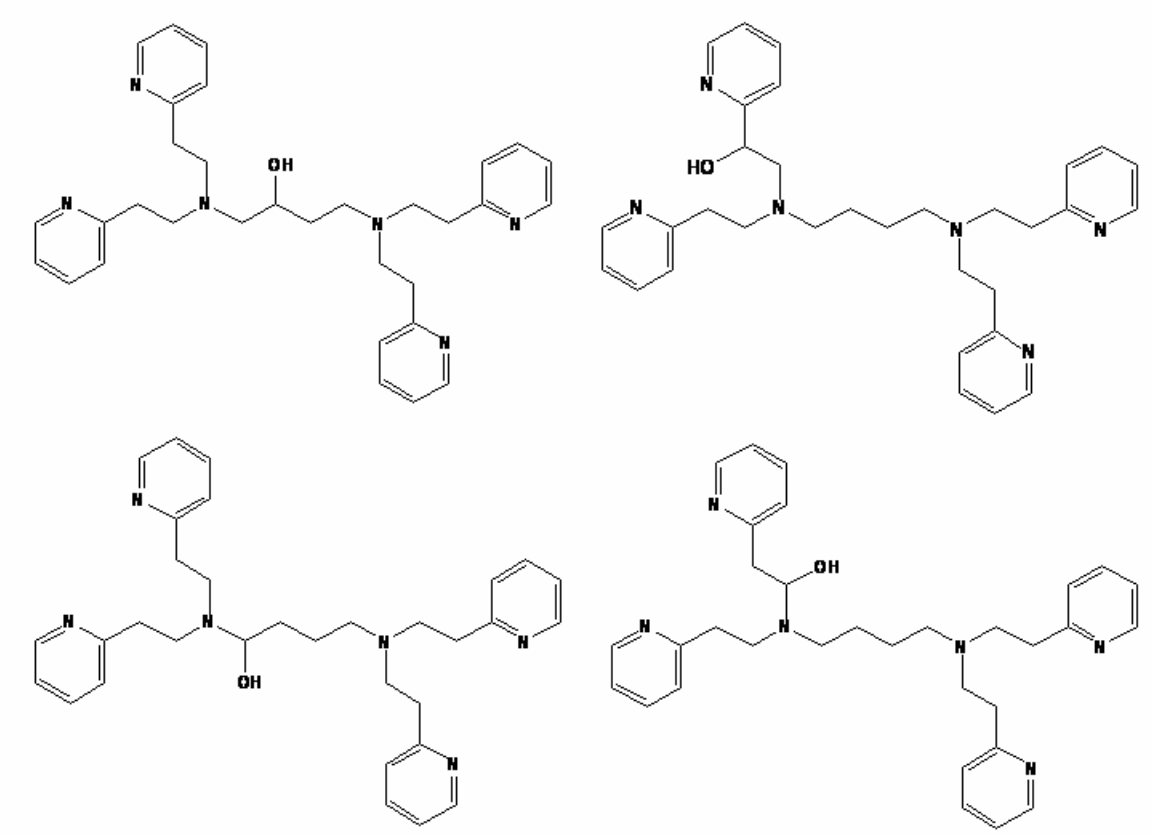

Figure S7. Four possible structure of the minor component I of ligand degradation products after $Cu^{II}_2\mathbf{N_4}$ reaction with H_2O_2. See text.

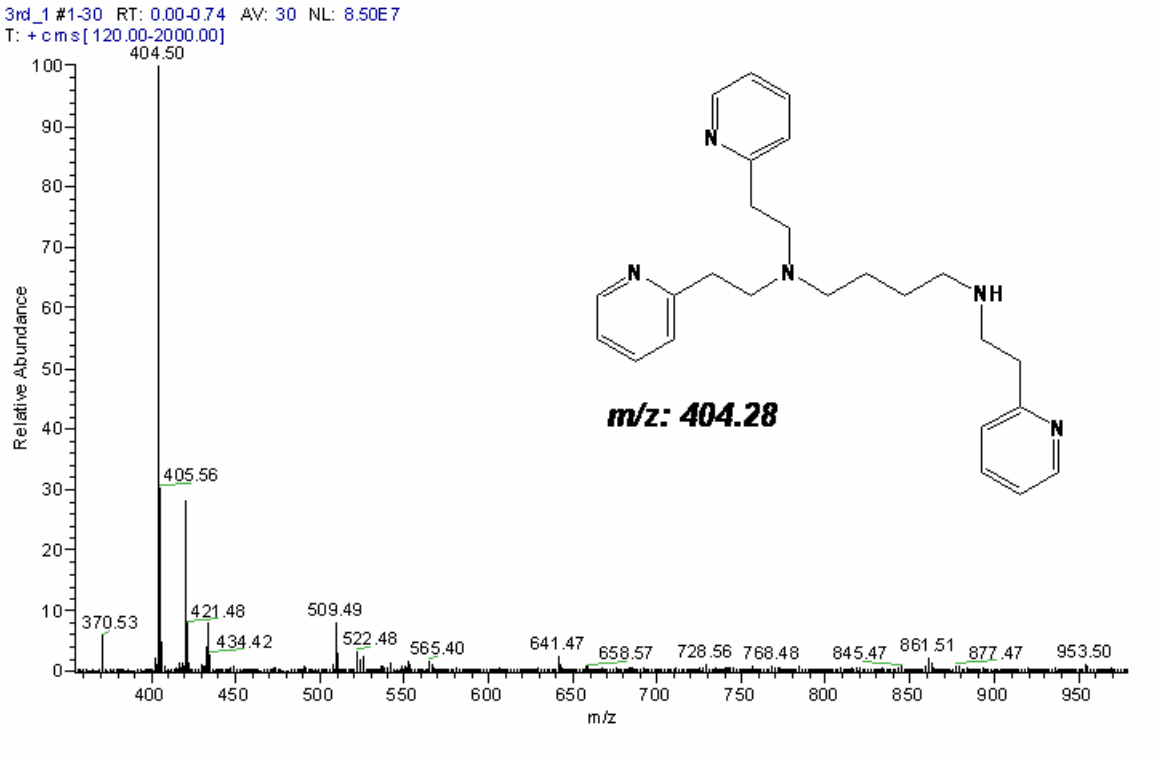

Figure S8. ESI-Mass spectrum of the minor component II of ligand degradation products after Cu^{II}_2**N4** reaction with H_2O_2. The insert indicates the likely structure derived from **N4** ligand oxidation, an oxidative N-dealkylation reaction

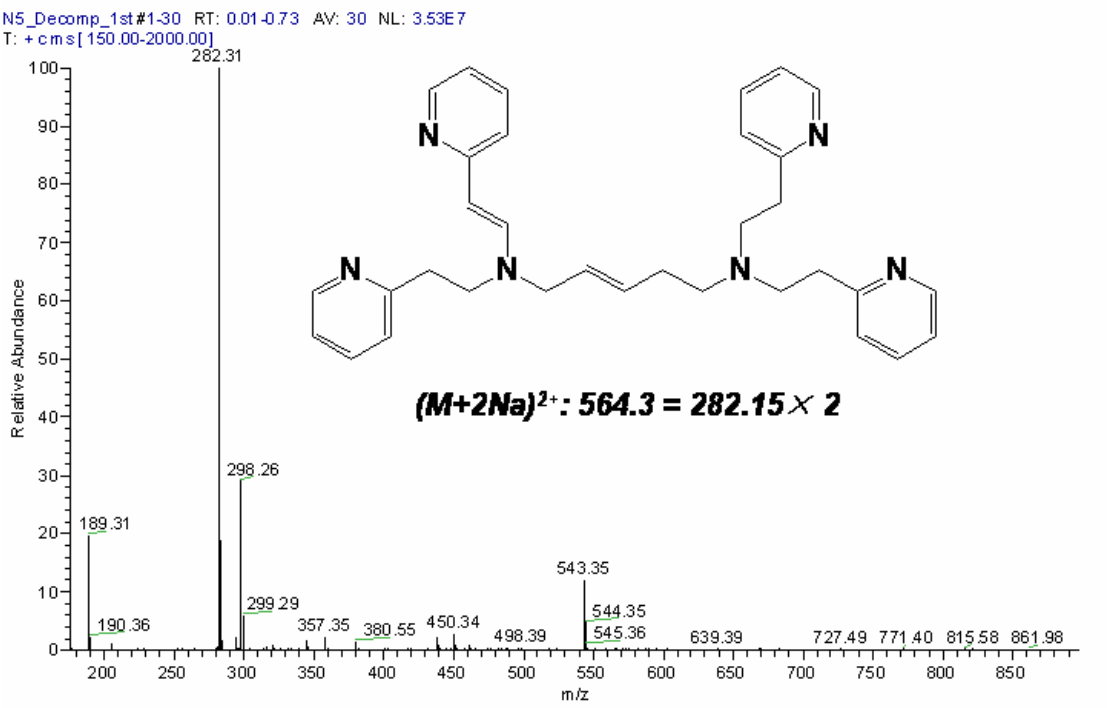

Figure S9. ESI-Mass spectrum of the major component of ligand degradation products after $Cu^{II}_2\mathbf{N_5}$ reaction with H_2O_2. The insert depicts the product structure assigned.

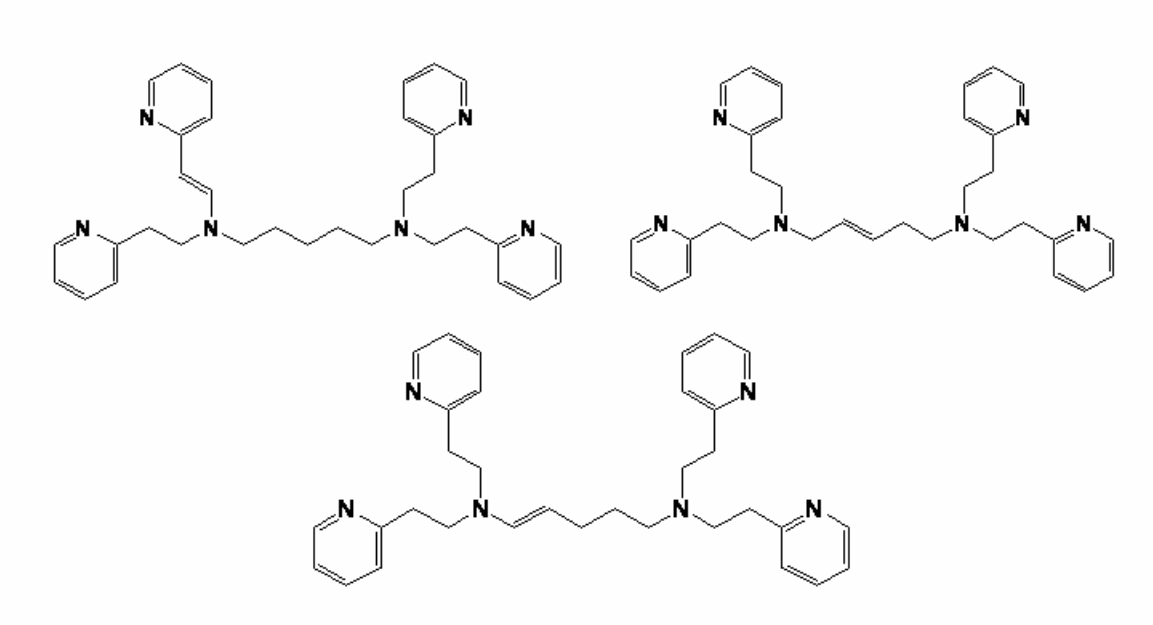

Figure S10. Based on ESI-MS data, we show three possible structures for the minor component of ligand degradation products after Cu^{II}_2**N5** reaction with H_2O_2.

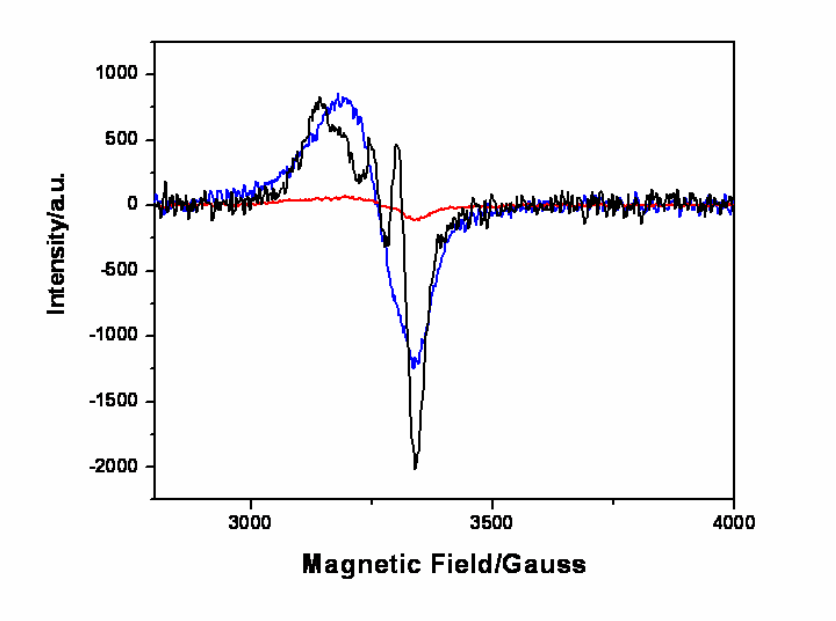

Figure S11. EPR spectra of for an aqueous solutions of $[Cu^{II}(TMPA)(H_2O)](ClO_4)_2$ (6.13 mM, black), $Cu^{II}_2\mathbf{N_4}$ (4.52 mM, blue) and $Cu^{II}_2\mathbf{N_4}$ after addition of H_2O_2 (red). The data indicate that for $Cu^{II}_2\mathbf{N_4}$, the Cu(II) ions in the complex behave independently, exhibiting mononuclear single-Cu ion behavior, while the (hydro)peroxide product complex is EPR silent, indicating a bridged species.

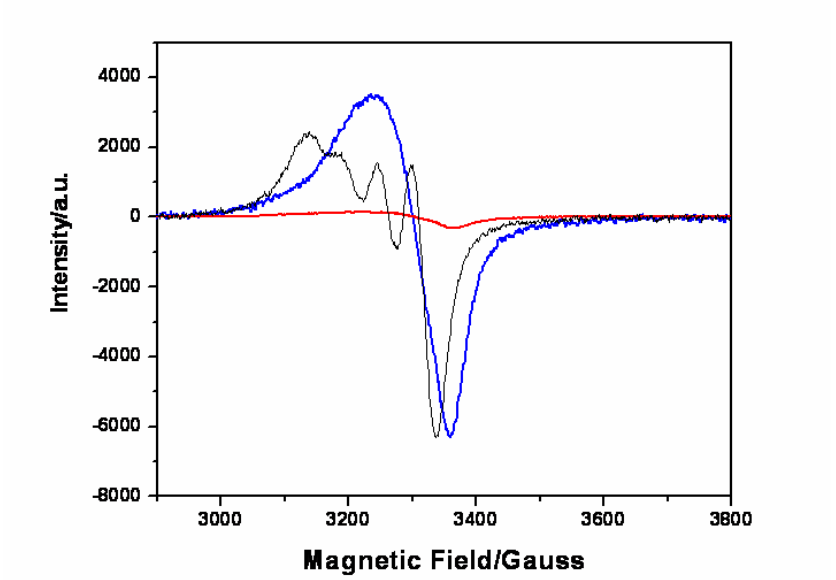

Figure S12. EPR spectra of for an aqueous solutions of $[Cu^{II}(TMPA)(H_2O)](ClO_4)_2$ (24.5 mM, black), $Cu^{II}_2\mathbf{N_5}$ (21.4 mM, blue)) and $Cu^{II}_2\mathbf{N_5}$ after addition of H_2O_2 (red). The data indicate that for $Cu^{II}_2\mathbf{N_5}$, the Cu(II) ions in the complex behave independently, exhibiting mononuclear single-Cu ion behavior, while the (hydro)peroxide product complex is EPR silent, indicating a bridged species.

References

1. Kieber, D.J.; Blough, N.V. *Anal. Chem.* **1990**, 62, 2275.
2. Vaughan, P. P.; Blough, N.V. *Environ. Sci. Technol.* **1998**, 32, 2947.
3. Thomas-Smith, T. E.; Blough, N.V. *Environ. Sci. Technol.* **2001**, 35, 2721.
4. Li, B; Gutierrez, P. L.; Blough, N.V. *Anal. Chem.* **1997**, 69, 4295.
5. Li, B; Gutierrez, P.L.; Blough, N.V. *Methods Enzymol.* **1999**, 300, 202.
6. Clever, H. L.; Yong, C. L. Eds., *IUPAC Solubility Data Series*, Vol. 27/28, Methane, Pergamon Press, Oxford, English, 1987.
7. Buxton, G.V.; Greenstock, C.L.; Helman, W.P.; Ross, A.B. *J. Phys .Chem. Ref. Data* **1988**, 17, 513.
8. Samuni, A; Goldstein, S.; Russo, A.; Mitchell, J. B.; Krishna, M. C.; Neta, P. *J. Am. Chem. Soc.* **2002**, *124*, 8719.
9. Unpublished value obtained from an independent competitive kinetics study.
10. Stevens, G. C.; Clarke, R. M.; Hart, E. J. *J. Phys. Chem.* **1972**, 76, 3863.
11. Oturan, M. A.; Pinson, J. *J. Phys. Chem.* **1995,** *99*, 13948.
12. Karlin, K. D.; Hayes, J. C.; Juen, S.; Hutchinson, J. P.; Zubieta, J., *Inorg. Chem.* **1982,** 21, 4106-4108.